Available online at www.sciencedirect.com
ScienceDirect
International Journal of Heat and Mass Transfer 50 (2007) 821–832
International Journal of HEAT and MASS TRANSFER
www.elsevier.com/locate/ijhmt

Numerical investigation of the thermal separation in a Ranque–Hilsch vortex tube

Smith Eiamsa-ard [a,1], Pongjet Promvonge [b,*]

[a] Department of Mechanical Engineering, Faculty of Engineering, Mahanakorn University of Technology, Bangkok 10530, Thailand
[b] Department of Mechanical Engineering, Faculty of Engineering, King Mongkut's Institute of Technology Ladkrabang, Bangkok 10520, Thailand

Received 23 December 2005; received in revised form 22 August 2006
Available online 31 October 2006

Abstract

The application of a mathematical model for the simulation of thermal separation in a Ranque–Hilsch vortex tube is presented in this paper. The modelling of turbulence for compressible, swirling flows used in the simulation is discussed. The work has been carried out in order to provide an understanding of the physical behaviors of the flow, pressure, temperature in a vortex tube. A staggered finite volume approach with the standard k–ε turbulence model and an algebraic stress model (ASM) is used to carry out all the computations. To investigate the effects of numerical diffusion on the predicted results, the second-order upwind (SOU) and the QUICK numerical schemes are used and compared with the first-order upwind and the hybrid schemes. The computations show that the differences of results obtained from using the various schemes are marginal. In addition, results predicted by both turbulence models generally are in good agreement with measurements but the ASM performs better agreement between the numerical results and experimental data. The computations with selective source terms of the energy equation suppressed show that the diffusive transport of mean kinetic energy has a substantial influence on the maximum temperature separation occurring near the inlet region. In the downstream region far from the inlet, expansion effects and the stress generation with its gradient transport are also significant.

Keywords: Ranque–Hilsch vortex tube; Thermal/temperature separation; k–ε model; ASM

1. Introduction

Vortex flows or swirl flows have been of considerable interest over the past decades because of their occurrence in industrial applications, such as furnaces, gas-turbine combustors and dust collectors (Gupta et al. [1]). Vortex (or high swirl) can also produce a hot and a cold stream via a Ranque–Hilsch vortex tube. The vortex tube has been used in industrial applications of cooling and heating processes because of a simple, compact, light and quiet (in operation) device [2,3]. The vortex tube is a mechanical device operating as a refrigerating machine by separating a compressed gas stream into a low total temperature region and a high one. Such a separation of the flow into regions of low and high total temperature is referred to as the temperature (or energy) separation effect. Generally, the vortex tube can be classified into two types. One is the counter-flow type (often referred to as the standard type) and the other the parallel or uni-flow type.

The vortex tube was first discovered by Ranque [4] but was revived and improved in efficiency by Hilsch [5]. Then, Hilsch's tubes and documents were studied extensively. Indicative of early interest in the vortex tube is the comprehensive survey by Westley [6] which included over one hundred references. Other literature surveys such as Dobratz [7] and Nash [8] provided extensive reviews of vortex tube applications and enhancements. Because of the multitude of the obscuring and interacting physical features involved, the actual flow in a vortex tube is very complex, involving recirculation, swirl and temperature separation, the

* Corresponding author. Tel.: +662 3264197; fax: +662 3264198.
E-mail address: kppongje@kmitl.ac.th (P. Promvonge).
[1] Tel./fax: +662 9883666x241.

0017-9310/$ - see front matter © 2006 Elsevier Ltd. All rights reserved.
doi:10.1016/j.ijheatmasstransfer.2006.08.018

Nomenclature

$C_{\varepsilon 1}$, $C_{\varepsilon 2}$	constants in the dissipation rate equation
C_v or C_p	specific heat
C_μ	constant in the k–ε model
D	diffusion term; dimension
D_0	tube diameter
G	stress generation
k	turbulence kinetic energy
K	mean kinetic energy
l, l_s	length scale, slot width
$\bar{p}$	mean pressure
r	radial co-ordinate, radius
R	radius of tube
S	general source term
t_{ij}	viscous stress tensor
$T_{ijk,k}$	net diffusive transport of stress
$T_{kk,k}$	net diffusive transport of TKE
$\tilde{u}, \tilde{v}, \tilde{w}$	Favre-averaged velocity in x-, r- and θ-directions

Greek symbols

β, λ	turbulence model constant
δ_{ij}	Kronecker delta tensor
ϕ	generalised dependent variable
Φ_{ij}	local pressure–strain term
Γ_ϕ	exchange coefficient
τ_{ij}	Reynolds stress tensor
θ	circumferential co-ordinate
ρ	density
σ_ϕ	Schmidt or Prandtl numbers for the scalar ϕ
ε	dissipation $= \varepsilon_s + \varepsilon_d$
ε_s, ε_d	solinoidal dissipation, compressible dissipation
μ, μ_t	dynamic viscosity, turbulent viscosity
μ_e	effective viscosity, $\mu_e = \mu + \mu_t$

Subscripts

e	effective
t	turbulence; total
s	static
i, j, k	Cartesian indices

Superscripts and overbars

$'$	fluctuating quantity in time-averaging
$''$	fluctuating quantity in Favre-averaging
—	mean quantity
$\sim$	Favre-average quantity

occurrence of which cannot be clearly described (Ahlborn et al. [9]). A few simple computational studies [10,11] for this kind of flow had been attempted before but all failed to predict satisfactorily its temperature variations and flow characteristics.

Recent efforts have successfully utilized computational fluid dynamics (CFD) modelling to explain the fundamental principles behind the energy separation produced by the vortex tube. Flohlingsdorf and Unger [12] studied on the phenomena of velocity and energy separation inside the vortex tube through the Code system CFX with the k–ε model. Promvonge [13] applied an algebraic Reynolds stress model (ASM) for the simulation of a strongly swirling flow in a vortex tube and found that the use of ASM results in more accurate prediction than the k–ε model. Behera et al. [14] investigated the effect of the different types and number of nozzles on temperature separation in a counter-flow vortex tube by ways of CFD and experiment. The modelling of the vortex tube was carried out using the code system, Star-CD with 'Renormalization Group' (RNG) version of the k–ε model. Aljuwayhel et al. [15] also studied the energy separation mechanism and flow phenomena in a counter-flow vortex using the CFD code FLUENT with the standard k–ε model and the RNG k–ε model. They reported that the RNG k–ε model provides better predictions and the vortex-tube flow field can be divided into three regions that correspond to: flow through the hot exit (hot flow region), flow through the cold exit (cold flow region), and flow within the device (re-circulating region). This is contrary to results of Skye et al. [16] claimed that for vortex tube's performance, the standard k–ε model performs better than the RNG k–ε model despite using the same commercial CFD code FLUENT. Some of these investigators tried to employ higher-order turbulence models but they could not get converged solutions due to numerical instability in solving the strongly swirling flows. Except for Promvonge [13], all the computations found in the literature used the first-order turbulence and simple heat flux models which are considered unsuitable for complex, compressible vortex-tube flows.

Computation of vortex flows is a difficult and challenging task. Large velocity gradients appear in these flows, so numerical problems and turbulence modelling play a crucial role in their analysis. The commonly used, the k–ε model may not be suitable for simulating swirling turbulent flows. The second-order moment closure models, i.e., the Reynolds stress model (RSM) and the algebraic Reynolds stress model (ASM) provide better methods for the simulation of swirling turbulent flows [17–19]. The RSM is regarded as a most logical approach to the turbulence closure problem, which does not need any ad hoc modification for extra strain rates. However, in the prediction of compressible swirling flows with the RSM, it is much extra computational effort to solve six Reynolds stress transport equations simultaneously and much attention needs to be paid to numerical stability and inlet boundary conditions. It is for this reason that a simplified algebraic Reynolds stress turbulence model in axisymmetric cylindrical co-ordinates

is developed and employed for simulating compressible vortex flows.

The specific objective of the present work is to formulate a space and time accurate numerical procedure for calculating 2D steady, axisymmetric, compressible swirling flows with thermal separation in a vortex tube. The starting point of the work is the "TEFESS" code developed by Pun [20] for general 2D flows. The present work has been built upon the above code, incorporating an algebraic Reynolds stress model (ASM) and other models involved. It is then used to simulate compressible subsonic flows in a vortex tube [21] to predict the flow characteristics and temperature separation. This appears to be the first extensive numerical investigation of a vortex-tube flow using the finite volume method together with a high-order turbulence model.

2. Mathematical formulation

2.1. Governing equations

For steady, compressible flows the Favre-averaged mean equations of motion, the turbulence kinetic energy (TKE) equation, the energy equation and the equation of state in Cartesian tensor notation can be summarised as

$$\frac{\partial}{\partial x_i}(\bar{\rho}\tilde{u}_i) = 0, \tag{1}$$

$$\frac{\partial(\bar{\rho}\tilde{u}_i\tilde{u}_j)}{\partial x_j} = -\frac{\partial \bar{p}}{\partial x_i} + \frac{\partial}{\partial x_j}\left(\bar{t}_{ij} + \tau_{ij}\right), \tag{2}$$

$$\frac{\partial}{\partial x_j}(\bar{\rho}\tilde{u}_j k) = \tau_{ij}\frac{\partial \tilde{u}_i}{\partial x_j} - \bar{\rho}\varepsilon + \frac{\partial}{\partial x_j}\left(\overline{t_{ji}u_i''} - \bar{\rho}\frac{1}{2}\,\widetilde{u_j''u_i''u_i''} - \overline{\rho' u_j''}\right) - \overline{u_i''}\frac{\partial \bar{p}}{\partial x_i} + \overline{p'\frac{\partial u_i''}{\partial x_j}}, \tag{3}$$

$$\frac{\partial}{\partial x_j}\left(\bar{\rho}\tilde{u}_j\tilde{E}\right) = \frac{\partial}{\partial x_j}\left(\overline{t_{ji}u_i''} - \overline{p'u_j''} - \bar{\rho}\frac{1}{2}\,\widetilde{u_j''u_i''u_i''}\right) - \frac{\partial}{\partial x_j}\left(\bar{q}_{L_j} + \bar{\rho}\,\widetilde{u_j''h''}\right) + \frac{\partial}{\partial x_j}(\tilde{u}_i(\bar{t}_{ij} + \tau_{ij})) - \frac{\partial}{\partial x_j}(\tilde{u}_j\bar{p}), \tag{4}$$

$$\bar{p} = \bar{\rho}R\tilde{T} = (\gamma - 1)(\bar{\rho}\tilde{E} - \bar{\rho}K - \bar{\rho}k). \tag{5}$$

In the preceding, an overbar indicates the mean relative to Reynolds averaging, with a single prime for fluctuation. A tilde and a double prime are corresponding ones for Favre averaging. Also, x_i are the coordinate directions, and ρ is density, u_i are the velocities in the three coordinates directions, k defined by $\bar{\rho}k = \frac{1}{2}\overline{\rho u_i'' u_i''} = \frac{1}{2}\bar{\rho}\,\widetilde{u_i''u_i''}$ is the turbulence kinetic energy, $\bar{p}$ is mean pressure, $\tilde{E} \equiv C_v\tilde{T} + \frac{1}{2}\tilde{u}_i\tilde{u}_i + \frac{1}{2}\,\widetilde{u_i''u_i''}$ is the mean total energy, $K \equiv \frac{1}{2}\bar{\rho}\tilde{u}_i\tilde{u}_i$ is the mean kinetic energy and γ is the ratio of specific heats (C_p/C_v). $\bar{q}_L$ is the mean heat flux and the mean viscous stress tensor is approximated as

$$\bar{t}_{ij} = \bar{\mu}\left(\frac{\partial u_i}{\partial x_j} + \frac{\partial u_j}{\partial x_i}\right) - \frac{2}{3}\bar{\mu}\frac{\partial u_k}{\partial x_k}\delta_{ij}. \tag{6}$$

Finally, $\tau_{ij} = -\overline{\rho u_i'' u_j''} = -\bar{\rho}\,\widetilde{u_i''u_j''}$ is the Favre-averaged Reynolds stress tensor. The mean conservation equations have resulted in additional terms: $\tau_{ij}, \overline{t_{ij}u_j''}, \overline{p'u_i''}, \bar{\rho}\,\widetilde{u_i''h''}$ and $\bar{\rho}\,\widetilde{u_j''u_i''u_i''}/2$ that require modelling. The modelling of some of the unclosed terms in these equations is based on their incompressible models whereas explicit compressible models are required for others. More details are found in Promvonge [22] on the various models used. In the present study, two turbulence closure models are used, namely the standard k–ε model and an algebraic stress model (ASM). The k–ε model has already been reviewed in many references such as Gatski [23], and Wilcox [24], and it will not be repeated here.

2.2. Algebraic Reynolds stress model (ASM)

For simplicity in solving the six Reynolds stresses, Rodi's approximation [25] is used in this study and the Reynolds stress transport can be expressed in algebraic form as follows:

$$\frac{D\tau_{ij}}{Dt} - T_{ijk,k} = \frac{\tau_{ij}}{\rho k}\left(\frac{Dk}{Dt} - T_{kk,k}\right). \tag{7}$$

Substitution of Reynolds and Favre-averaged transport and the TKE equations into Eq. (7) gives the desired algebraic expression for τ_{ij}:

$$\frac{\tau_{ij}}{\bar{\rho}k}\left(G - \bar{\rho}\varepsilon - \overline{u_i''}\frac{\partial \bar{p}}{\partial x_i} + \overline{p'\frac{\partial u_i''}{\partial x_k}}\right) = G_{ij} + \Phi_{ij} - \frac{2}{3}\delta_{ij}\bar{\rho}\varepsilon + \frac{2}{3}\overline{p'\frac{\partial u_k''}{\partial x_k}} - \overline{u_i''}\frac{\partial \bar{p}}{\partial x_j} - \overline{u_j''}\frac{\partial \bar{p}}{\partial x_i} + \overline{u_i''}\frac{\partial \bar{t}_{jk}}{\partial x_k} + \overline{u_j''}\frac{\partial \bar{t}_{ik}}{\partial x_k}, \tag{8}$$

in which G_{ij} is local production of Reynolds stress, Φ_{ij} is local pressure strain and ε is the TKE dissipation rate. The ASM expressions, after modelling of the unclosed terms, with the pressure dilatation ($\overline{p'\partial u_k''/\partial x_k}$) and the average fluctuating velocity ($\overline{u_i''}$) terms neglected can thus be written as

$$-\tau_{ij} = \overline{\rho u_i'' u_j''} = \frac{2}{3}\delta_{ij}\bar{\rho}k + \frac{\lambda k}{\varepsilon}\left(G_{ij} - \frac{2}{3}\delta_{ij}G - \beta A_{ij}\right), \tag{9}$$

where the empirical constants λ and β, introduced to represent the effect of fluid swirling on gas turbulence, were found to be 0.135 and between 0.0 and 2.2, respectively. The above implicit ASM expressions can be simplified to obtain an explicit set for easy solution as proposed by Zhang et al., [26] and Nieh and Zhang [27] for application to a strongly swirling flow. Thus, the above ASM for 2D steady compressible flows have been formulated and incorporated in an existing "TEFESS" code developed by Pun [20].

2.3. Common form for the equations

All the governing partial differential equations can be reorganised and expressed in a standard form that includes

the convection, diffusion, and source terms for 2D axisymmetric flows as follows:

$$\frac{\partial}{\partial x}(\bar{\rho}\tilde{u}\phi)+\frac{1}{r}\frac{\partial}{\partial r}(r\bar{\rho}\tilde{v}\phi)-\frac{\partial}{\partial x}\left(\Gamma_{\phi x}\frac{\partial\phi}{\partial x}\right)-\frac{1}{r}\frac{\partial}{\partial r}\left(r\Gamma_{\phi r}\frac{\partial\phi}{\partial r}\right)=S_{\phi}, \tag{10}$$

where ϕ, $\Gamma_{\phi x}$, $\Gamma_{\phi r}$ and S_{ϕ} represent the generalised variables, the exchange coefficients in x and r directions and the source terms, respectively.

2.4. Solution procedure

In the present computation the Favre-averaged Navier–Stokes equations, Eqs. (1) and (2); the TKE equation, Eq. (3); the energy equation, Eq. (4); the equation of state, Eq. (5); the TKE dissipation rate equation, are to be solved numerically by a finite-volume method together with the turbulence model equations, Eq. (9) for the ASM. The SIMPLE algorithm is utilised for pressure–velocity de-coupling and iteration [28]. The discretization of the governing equations is accomplished by means of the upwind, the hybrid, the second-order upwind (SOU) and the quadratic upstream interpolation for convective kinematics (QUICK) [29] schemes and the source term linearisation on a staggered grid cell. The under-relaxation iterative TDMA line-by-line sweeping technique is used for solving the resultant finite-difference equations. Due to the highly non-linear and coupling features of the governing equations for swirling flows, lower under-relaxation factors ranging from 0.001 to 0.2 are chosen for the three velocity components to ensure that the stability and convergence of the iterative calculation. Wall function [20] was used at the grid nodes along the walls.

3. The vortex tube of Hartnett and Eckert [21]

The vortex tube of Hartnett and Eckert [21] was chosen to study the flow characteristics and temperature separation. Since the purpose of the experiment, similar to the present study, was to obtain a detailed knowledge of the temperature and flow fields in a vortex type flow, the study was restricted to a vortex which was generated at the nozzle cross section before proceeding in one main direction down the tube through the exit at the far end of the tube. The orifice of the tube was completely closed. Measurements were made in a 0.0762 m diameter Plexiglas tube of 0.77 m length. The air entered the tube tangentially through eight nozzles of 0.009525 m diameter each, equally spaced around the circumference of the tube and left the tube through a 60° cone-shaped valve. This geometry was designed to preserve flow symmetry. Experimental velocity, pressure and temperature profiles were provided at 3 axial locations, namely $x = 0.0254$, 0.1524 and 0.4572 m (or $x/D_0 = 0.333$, 2 and 6, respectively) from the nozzle, with the inlet nozzle pressure (p_0) at approximately 2.3 atm (abs.). Measurements were made by using pitote tube probes. Total temperature, total pressure and static pressure profiles were measured directly whereas the velocity and the static temperature profiles were obtained by calculations from the other measured data. Details of the geometry and fluid properties are listed in Table 1.

Table 1
Data for the vortex flow of Hartnett and Eckert [21]

Tube characteristics	
Tube length, L (m)	0.77
Tube diameter, D_0 (m)	0.0762
No. of nozzles at the inlet	8
Nozzle diameter, d_n (m)	0.009525
Cone valve opening	0.007854
L/D_0 ratio	10.1
Inlet fluid properties	
Fluid	Air
Temperature, T_{in} (K) (approx.)	297
Supply pressure before nozzle, p_0, (Pa) (gage)	1.374×10^5
Inlet flow conditions	
Mass flow rate, $\dot{m}_{in}$ (kg/s)	0.2184

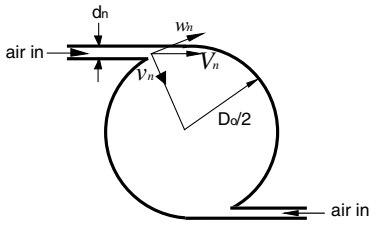

Fig. 1. Inlet properties of the vortex tube.

The computational domain of the vortex-tube flow system is illustrated in Fig. 2a while Fig. 2b shows a 50×25 non-uniform grid distribution used for this case. Calculations with both the standard k–ε model and the ASM were performed with different numerical schemes. Input data

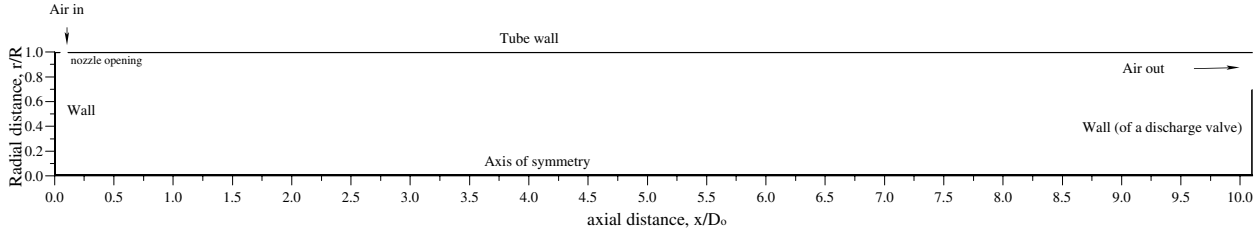

Fig. 2a. Computational domain of the flow system in vortex tube of Hartnett and Eckert [21].

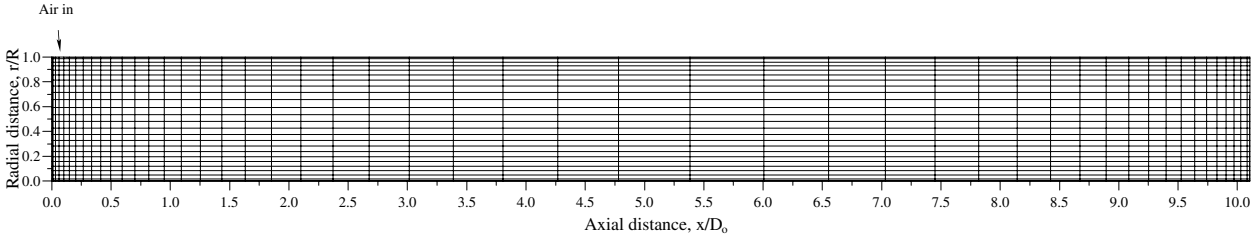

Fig. 2b. Grid distribution (50 × 25).

Table 2
Input data for Hartnett and Eckert's tube

V_n (m/s)	w_n (m/s)	v_n (m/s)	ρ_n (kg/m^3)	T_n (K)	l_s (m)	Mach no. (M_{in})
230	210	94	1.68	297	0.0058	0.69

values needed in the present calculation are given in Table 2. In Table 2, the values of V_n and w_n were extrapolated from the experimental profiles while the other values were obtained from the procedure as described below.

4. Boundary conditions

The calculated mean quantities are compared with available measurements at selected stations. Basic assumptions for all the computations of the particular vortex-tube flow are made as follows: 2D axisymmetrical, subsonic flow inside the vortex tube, uniform flow properties at the inlet and ideal gas. Since the system is assumed to be an axisymmetric flow, only half of the flow domain needs to be considered throughout and special treatment for the flow at the inlet must be made for the computations. At the inlet, a circumferential slot is assumed instead of the actual inlet nozzles. For simplicity in the present computation the cone-shaped valve used as a discharge valve at the exit is replaced with a block valve. In addition, owing to lack of wall temperature information, the influences of the wall temperature on the predictions are investigated. Because of the complex geometry of the flow, data for boundary conditions should be carefully considered in order to make computations realistic. Details of data for the vortex-tube flow are given next.

4.1. Inlet

Properties at the inlet are usually obtained from experimental data, analysis, or estimated. It is very rarely that all the boundary conditions required are available from experiment. Quantities of primary importance here are the velocity components normal and tangential to the inlet. In axisymmetric flows, the swirl component must also be known. Compressed gas enters the vortex tube tangentially through one or more nozzles. Most experiments provide inlet data such as pressure p_0, temperature T_0 and mass flow rate just before the nozzle. Unfortunately, they cannot be used as input data for computations which need the data at the nozzle exit stage. Little is known about the static pressure p_n, temperature T_{in}, and velocity V_n, at the nozzle outlet. Those values may be obtained by extrapolation from their experimental profiles inside the tube to the nozzle exit location. Thus, this practice is adopted for the velocities; the total temperature at the nozzle exit is obtained by assuming an adiabatic nozzle, so that the total energy is conserved throughout the nozzle. Note that the static pressure values inside the flow field are calculated relative to the value at a reference point, for which measurement is available. Density at the inlet is calculated from the continuity equation:

$$\rho_n = \frac{\dot{m}_{in}}{A_n V_n}, \tag{11}$$

where A_n, ρ_n and V_n are the total area, density and average velocity at the nozzle exit respectively and $\dot{m}_{in}$ represents the total air mass flow rate. However, in the case where the total mass flow rate is not available but the static pressure and the static temperature profiles inside the tube are provided, the equation of state is used to estimate the density at the inlet ($\rho_n = p_s/RT_s$), the inlet static pressure and temperature used in the equation being obtained by extrapolation from the experimental profiles.

For axisymmetric flow, a circumferential slot at the inlet is used instead of the nozzle (or nozzles). The equivalent width of the slot, l_s, is calculated from the conservation of mass with the relation below.

$$l_s = \frac{\dot{m}_{in}}{\pi D_0 \rho_n v_n}, \tag{12}$$

where l_s, D_0 and v_n are the slot width, the vortex-tube diameter and the inlet radial velocity, respectively (as seen in Fig. 1).

From velocity triangle in Fig. 1:

$$v_n = \sqrt{V_n^2 - w_n^2}, \tag{13}$$

in which w_n is the tangential velocity at the inlet. The values of V_n and w_n in the present computations are obtained by extrapolation from experimental measurements.

The speed of sound, c, at the inlet, from $c = \sqrt{\gamma p_{in}/\rho_{in}}$ where p_{in} was extrapolated from measurements, is about 331 m/s. Therefore the inlet Mach number is 0.69, suggesting that the flow in the tube is subsonic and compressible.

The dynamic viscosity generally is a function of the temperature. However, in the present computations, it is assumed to be uniform throughout (equal to μ at the inlet temperature) because the temperature change in the vortex tube is not large.

4.2. Wall

The measurement selected was given without reference to the environment of the tube and it is believed that invariably the tube was exposed without insulation to the ambient temperature during the experimental investigation. Since the vortex tube was made of Plexiglas whose properties offered some insulation, the correct wall temperature should lie between the adiabatic wall and constant ambient temperatures. Therefore, both options of the wall temperature conditions were used by consideration with available measurements at given stations for comparison and the better one is selected.

4.3. Outlet

For simplicity in the present computation the cone-shaped valve used as a discharge control valve at the exit is replaced with a block valve for this flow. The conventional setting of zero gradient conditions was adopted for all variables except the axial velocity $\tilde{u}$, which is subject to continuity constraints. The error of energy balance between the input and the output energies is kept to be less than 3% for the constant wall temperature condition.

5. Results and discussion

5.1. Flow and temperature fields

First, the influence of grid size on the solution was investigated with two grid densities of 50×25 and 70×30 using the hybrid scheme and both the turbulence models. The effects of the grid densities on the total temperature and tangential velocity profiles at three downstream stations, namely, $x/D_0 = 0.333$, 2 and 6, are shown in Figs. 3a and 3b for the k–ε model and the ASM, respectively. It is seen that both the grid sizes give solutions very close to each other, indicating that a grid of 50×25 or finer would lead to results which were sufficiently grid-independent.

The effects of numerical schemes on the ASM results are examined with a grid of 50×25 and presented in Fig. 4, respectively. It is found that, except for some differences at the first station, all four schemes yield similar results. A closer examination at the first station reveals that the use of the SOU or the QUICK scheme leads to under-predicted results at the core, especially near the inlet region, and to slightly over-predicted results close to the wall when compared with the experimental data. Therefore, the use of a first-order numerical scheme, either the upwind or hybrid scheme is considered to be sufficient to give an accurate result in the present computation.

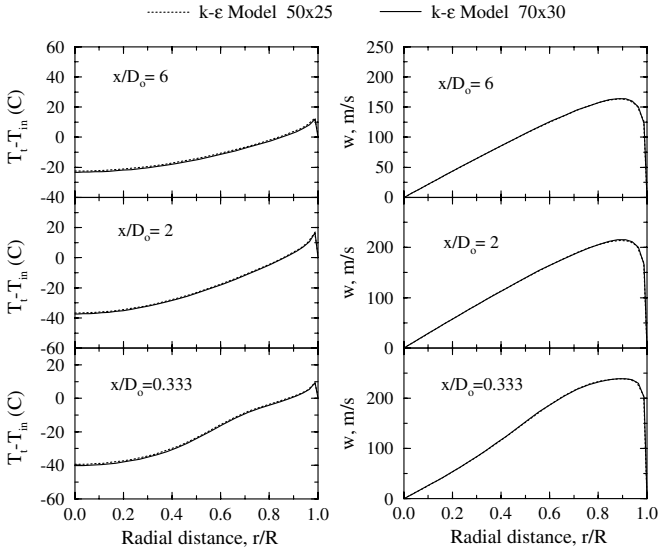

Fig. 3a. Sensitivity of grid densities to total temperature and tangential velocity profiles for the k–ε model.

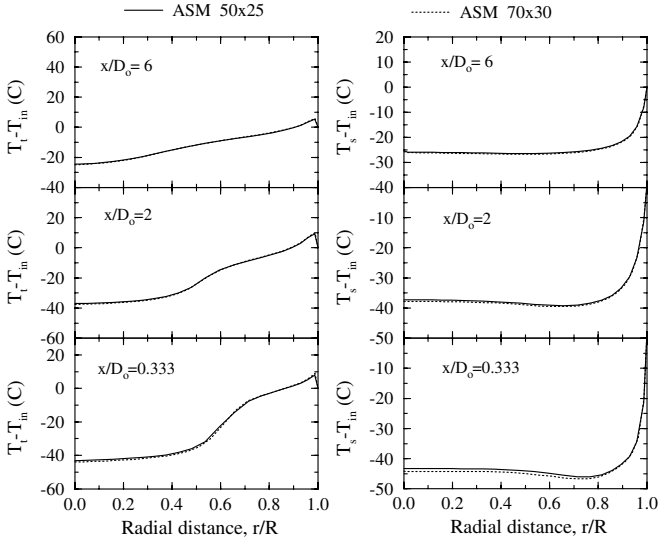

Fig. 3b. Sensitivity of grid densities to total temperature profiles for the ASM.

The effects of β between 0.0 and 0.6 on the total temperature and tangential velocity for the ASM are demonstrated in Fig. 5. It is found that the use of high β values can improve slightly the results near the wall but leads to under-predicted solutions in the core region. The optimum value for β based on the velocity profiles, should be in a range from 0.0 to 0.1. Since the β term originally came from the non-gradient convection terms arising from the transformation to the cylindrical co-ordinate system, this also points out that there is little effect of the convection terms.

Fig. 6(a) and (b) show, respectively, contour plots of the predicted static temperature for the k–ε model and the ASM; contours of the total temperature are, respectively, presented in Fig. 7(a) and (b). It is seen that, for static

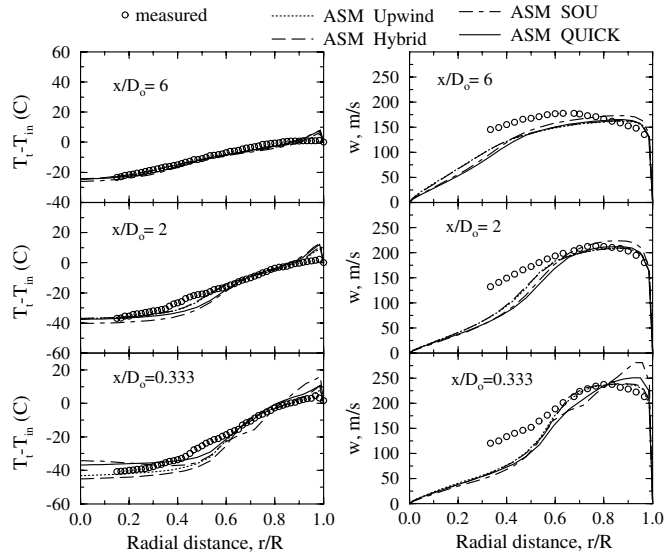

Fig. 4. Effects of numerical schemes on total temperature and tangential velocity profiles for the ASM with measurements of Hartnett and Eckert [21].

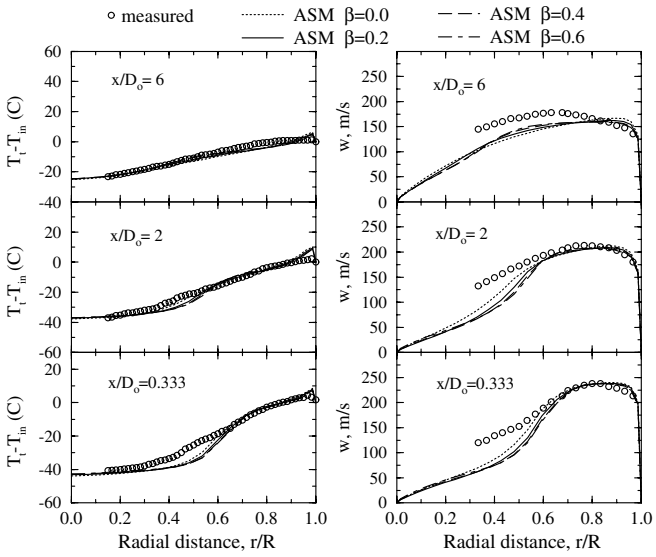

Fig. 5. Effects of β on predicted total temperature and tangential velocity profiles.

temperature contours in Fig. 6, temperature gradients are high in the region near the tube wall ($r/R > 0.6$) and are small in the core region of $r/R < 0.6$. The static temperature variations across the tube are seen to be considerably smaller than those found for the total temperature. It is of interest to note that the entire flow, except for the outer annular ring $r/R > 0.85$, is at a total temperature lower than the inlet temperature, T_{in}. The separation of the total temperature field into regions of high energy (high total temperature) along the tube wall and low energy is evident in Fig. 7 which shows that the total temperature is a minimum in the central region. The separation effect or temperature difference for the total temperature is large near the core of the inlet region and decreases as the exit is approached. The maximum total temperature in the field is visible at the axis location of $x/D_0 = 0.75$ for the k–ε model contours (Fig. 7(a)). For the ASM contours the peak one lays in a range of $x/D_0 = 0.0$ to $x/D_0 = 0.85$. This location of the maximum total temperature is confirmed by

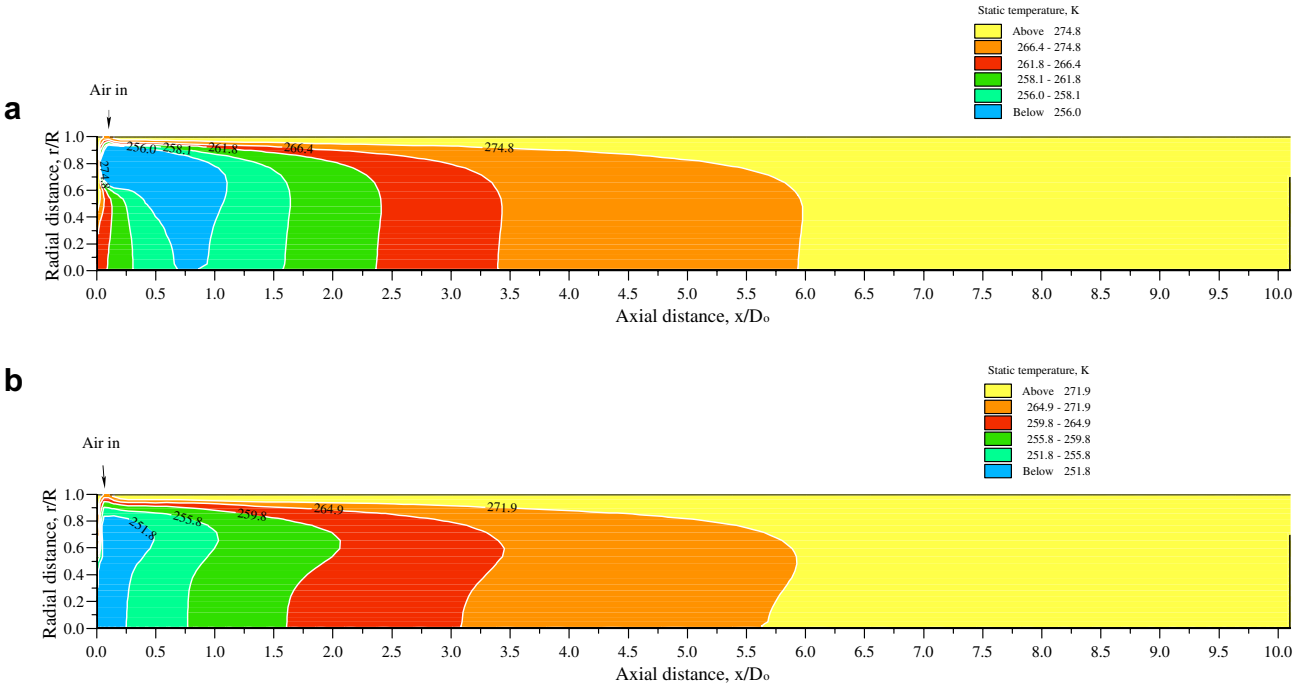

Fig. 6. Contours of static temperature predicted by (a) the k–ε model and (b) the ASM for vortex tube of Hartnett and Eckert [21].

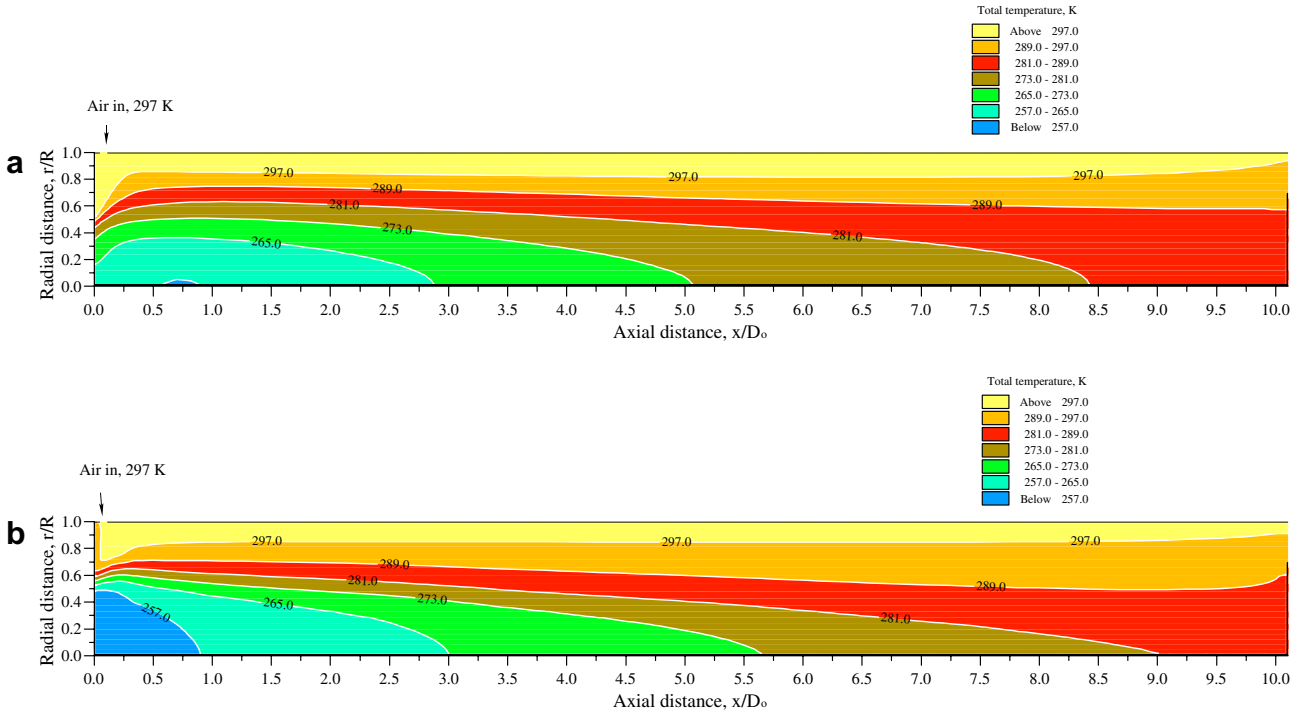

Fig. 7. Contours of total temperature predicted by (a) the k–ε model and (b) the ASM for vortex tube of Hartnett and Eckert [21].

measurements of Blatt and Trusch [30] who reported that the maximum temperature appears at the axis between $x/D_0 = 1.0$ and $x/D_0 = 1.5$

5.2. Analysis of temperature separation

To understand the temperature separation process in the vortex tube, further study is conducted by considering each of the source terms in the energy equation to find out which term plays a more crucial role on the temperature separation. The analysis of temperature separation in a vortex tube starts with the total energy equation, Eq. (4), which can be written, after its unclosed terms were modelled as

$$\underbrace{\frac{\partial}{\partial x_j}\left(\bar{\rho}\tilde{u}_j\tilde{E}\right)}_{\text{(I)}} - \underbrace{\frac{\partial}{\partial x_j}\left(\frac{\mu_e}{\sigma_E}\frac{\partial \tilde{E}}{\partial x_j}\right)}_{\text{(II)}} = \underbrace{\underbrace{\left(\bar{t}_{ij}+\tau_{ij}\right)\frac{\partial \tilde{u}_i}{\partial x_j}}_{a} + \underbrace{\tilde{u}_i\frac{\partial}{\partial x_j}\left(\bar{t}_{ij}+\tau_{ij}\right)}_{b}}_{\text{(III)}} - \underbrace{\frac{\partial}{\partial x_j}\left(\frac{\mu_e}{\sigma_E}\frac{\partial K}{\partial x_j}\right)}_{\text{(IV)}} - \underbrace{\frac{\partial}{\partial x_j}\left(\tilde{u}_j\bar{p}\right)}_{\text{(V)}}. \tag{14}$$

In Eq. (14), from left to right, the five terms are:

(I) the net convection of total energy by the mean flow,
(II) the net diffusion of total energy,
(III) the turbulent dissipation and viscous heating, which comprises the stress generation (IIIa) and stress gradient transport (IIIb),
(IV) the net diffusive transport of mean kinetic energy, and
(V) the expansion effects or pressure work.

It is interesting to note that the formulation of the mean energy equation in this way has yielded a diffusive transport of mean kinetic energy which does not show up explicitly in other modelled forms of the energy equation. In the standard format, the first and second terms of Eq. (14) are the convection and diffusion terms respectively and the three terms on the right-hand side are the source terms. This arrangement makes the computations realistic since physically the convection and the diffusion processes occur simultaneously in the flow fields. The vortex tube of Hartnett and Eckert [21] was chosen because of completely available experimental data. Furthermore, the assumption of axisymmetrical flow made in the present computations was more reasonable since multiple nozzles at the inlet were used for the vortex-tube flow.

The computations were carried out with only the ASM due to its better performance over the k–ε model. Since the wall temperature boundary condition of the flow was not known, both the constant wall temperature (assumed to be at the ambient temperature) and the adiabatic wall were considered. It is worth noting that predictions with each of the source terms in the energy equation do not make significant differences to the flow fields which are omitted here and only the temperature field for the vortex-tube will be discussed.

Figs. 8 and 9 compare the predicted radial profiles of the total and static temperatures using different source terms in the energy equation with measurements of Hartnett and

Eckert [21] at three downstream locations for the constant wall temperature and the adiabatic wall conditions respectively. It should be borne in mind that the convection and diffusion terms were included for all computations and the source terms were suppressed selectively. Furthermore, the experimental profiles of static temperature were not measured directly but obtained by calculation from the isentropic relation, as has been discussed before.

5.2.1. Effect of the convection and diffusion of total energy (zero source term)

Total temperature. Figs. 8(a) and 9(a) show that, for both the wall conditions, the calculation without any source term in the energy equation leads to no temperature separation and the total temperature throughout the tube is uniform. This indicates that the energy separation effect in the tube must be due to one or more of the source terms.

Static temperature. Figs. 8(b) and 9(b) show that there is a difference of static temperature in the inner region and in the outer region, for both wall conditions. The difference of the temperature between the two regions is large near the inlet region and gradually decreases in the downstream region. This suggests that there is an outward heat flux along the radial direction caused by the static temperature difference of the inner and outer gas layers. This heat current from the static temperature gradient makes the total temperature uniform throughout the tube.

5.2.2. Effect of expansion effects or pressure work (term V)

Total temperature. Predictions with the pressure work source term (term V) of the energy equation for both the wall conditions show a slight increase in the total temperature at the first station, $x/D_0 = 0.333$, but then a gradual drop in total temperature can be seen at the last two stations as evident in Figs. 8(a) and 9(a). This indicates that the pressure work would rather reduce than enhance the vortex thermal separation effect in the vicinity of the inlet where maximum energy separation takes place, but significant influence of the expansion effects on the thermal separation is found in the far downstream locations.

Static temperature. It appears that the static temperature profiles for both the wall conditions are similar to those

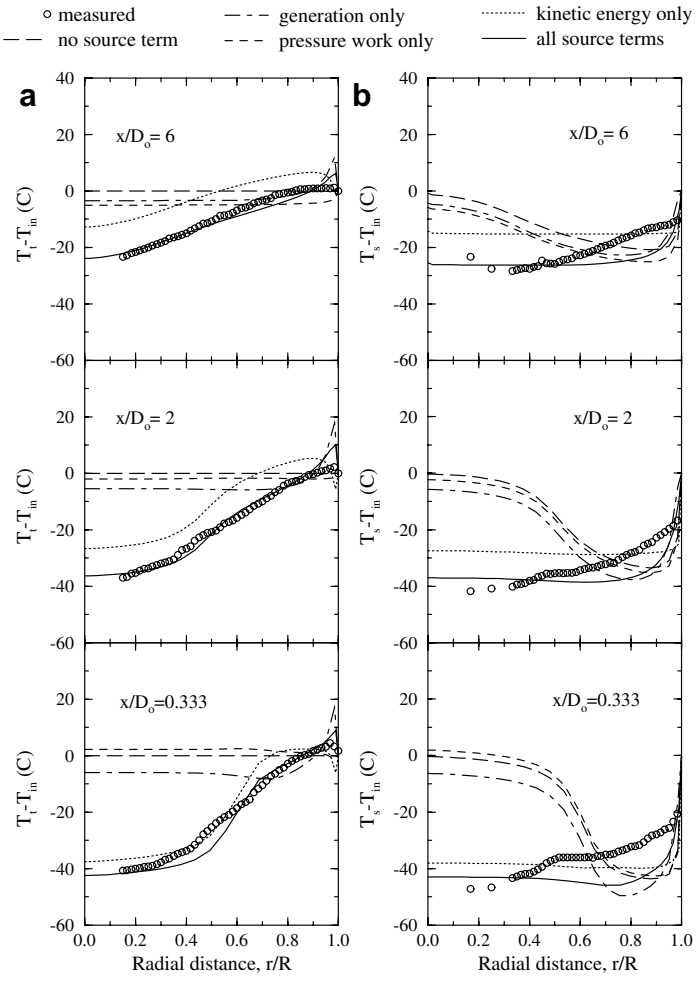

Fig. 8. Effect of source terms in the energy equation on temperature separation for constant wall temperature condition in the vortex tube of Hartnett and Eckert [21], (a) total temperature and (b) static temperature.

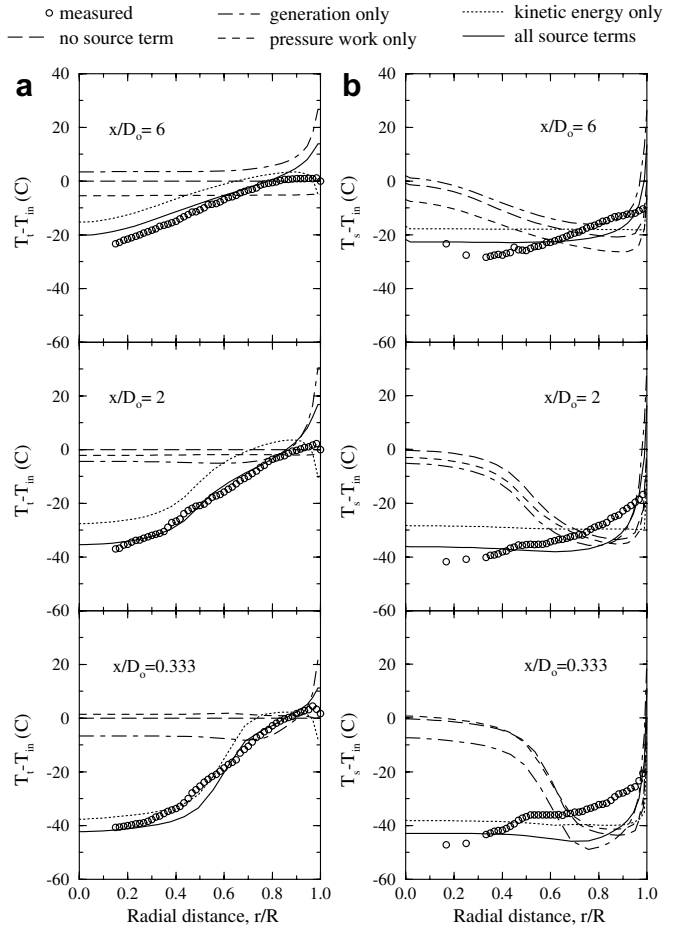

Fig. 9. Effect of source terms in the energy equation on the temperature separation for adiabatic wall condition in the vortex tube of Hartnett and Eckert [21], (a) total temperature and (b) static temperature.

with the zero source term but are at a slightly higher temperature level for the first station and at a lower temperature level for the downstream locations. This shows that the pressure work source term effect leads to a slight increase in static temperature in the inlet region and it then decreases gradually as exit is approached. The heat flux arising from the static temperature difference between the inner and outer region is due to the zero source term case, not from this source term.

5.2.3. Effect of the stress generation and gradient transport (term III)

Total temperature. The use of the stress generation (or production) term and stress gradient transport (term III) as the only energy source term, for the constant wall temperature condition, results in a temperature drop in the central region and a temperature increase in the near wall region ($r/R > 0.9$) for all three stations, Fig. 8(a). This can be attributed to a high level of shear stresses due to friction in the near wall region. The temperature separation effect is large at the first station; it gradually decreases in the far downstream locations. For the adiabatic wall condition, the temperature separation is similar to the case of constant wall temperature for the first station but decreases faster than those of the constant wall temperature case for the last two stations as can be seen in Fig. 9(a). It is clear that the low temperature separation occurring when the adiabatic wall condition is applied, is due to the stress production and gradient transport effect for this flow case.

Static temperature. It is seen from Figs. 8(b) and 9(b) that the static temperature profiles show a similar trend with those for the zero source term case but are at a lower temperature level for the constant wall temperature condition. The profiles of the adiabatic wall condition case also shift below from those with the zero source term except for the last station. This suggests that the stress production and gradient transport source terms result in a drop in static temperature in the inlet region. The heat flux from the temperature difference between the inner and outer region is mostly due to the convection and diffusion effect (zero source term). The effect of the stress production and gradient transport on the temperature separation is found to be fairly significant as can be seen in the total temperature profiles.

5.2.4. Effect of the mean kinetic energy diffusion (term IV)

Total temperature. The predictions with only the mean kinetic energy diffusion (term IV) as the source term in the energy equation show a considerable drop in total temperature in the central region, for both wall conditions. Close to the inlet, the total temperature profiles in the central region are close to those with all source terms included or the measurements, Figs. 8(a) and 9(a). At further downstream locations, the profiles are still similar to measurements but are at a higher temperature level. In the outer region ($r/R > 0.9$), a temperature drop appears in order to compensate the high temperature near the wall caused by the stress production and friction effects. Therefore, it is obvious that the mean kinetic energy diffusion is the main influence on the maximum temperature separation effect in the inlet region while in the downstream region the pressure work or expansion effects and the stress generation with its gradient transport are also fairly significant.

Static temperature. It is clear from Figs. 8(b) and 9(b) that the mean kinetic energy diffusion results in the uniform static temperature distribution across the radius of the tube except near the wall. The figures show that there is no heat flux from the static temperature difference for this source term except in the region very close to the tube wall. This suggests that the heat flux arising from the temperature difference for the zero source term case is absorbed and converted into mean kinetic energy by the diffusion process. The static temperature is seen to be the same as the total temperature along the tube axis for both wall conditions.

5.2.5. Effect of all the source terms

Total temperature. It is seen from Figs. 8(a) and 9(a) that when all source terms in the energy equation are included,

the total temperature profiles in the central region are similar to those obtained by the diffusion of mean kinetic energy for both wall conditions, but are at a lower temperature level. The profiles agree very well with measurements and the minimum temperature is well predicted.

Static temperature. Figs. 8(b) and 9(b) show that the static temperature is nearly uniform in the radial direction across the tube and there is a slight decrease in the temperature in the radially outward direction. This suggests that the small heat flux from the temperature difference moves from the central region to the outer region.

From the results and discussion, it is seen that each of the source terms in the energy equations shows the effect on the vortex thermal separation in the vortex-tube. The maximum temperature separation in a vortex tube, which is in the inlet region, mainly takes place from the diffusion of mean kinetic energy.

6. Conclusions

Numerical computations have been carried out to predict compressible vortex-tube flow using the k–ε model and the ASM. The present numerical results for the vortex-tube flows are compared with experimental data. Major findings can be summarised as follows:

- The ASM was employed due to its better performance. The computations show that mean kinetic energy diffusion is the main influence on the temperature separation effect occurring at the central axis near the inlet region, while in the far downstream region expansion effects (or pressure work), stress generation and stress gradient transport play also a significant effect.
- The gas leaving the inlet nozzle at high velocity creates a rapidly spinning vortex in the tube. The static temperature of the gas near the inlet is decreased substantially by the mean kinetic energy diffusion process and a little enhancement of the stress production with its gradient transport and the expansion effects. The static and total temperatures are nearly the same along the centre-line of the tube. This indicates that total temperature is very low at the axis. The convection and diffusion of total energy produces slight outward static temperature gradients along the radial direction, leading to small heat flux to the outer region. Far from the inlet, the expansion effects and the stress production play an important role to help increase the energy separation in the tube in addition to the diffusion transport of mean kinetic energy.

Acknowledgements

The author would like to gratefully acknowledge Dr. W.M. Pun and Prof. S. Sivasegaram for valuable discussion of this research.

References

[1] A.K. Gupta, D.G. Lilley, N. Syred, Swirl Flows, Reading, Abacus Press, Turnbridge Wells, England, 1984.
[2] T.J. Bruno, Applications of the vortex tube in chemical analysis, Process Control Quality, 3, Elsevier Science Publishers B.V., Amsterdam, 1992, pp. 195–207.
[3] T.J. Bruno, Applications of the vortex tube in chemical analysis. Part I: Introductory principle, Am. Lab. 25 (1993) 15–20.
[4] G.J. Ranque, Experiments on expansion in a vortex with simultaneous exhaust of hot air and cold air, Le Journal de Physique et le Radium (Paris) 4 (1933) 112–114. Also translated as General Electric Co., Schenectady Works Library, T.F. 3294 (1947).
[5] R. Hilsch, The use of expansion of gases in a centrifugal field as a cooling process, Rev. Sci. Instrum. 18 (2) (1947) 108–113.
[6] R. Westley, A Bibliography and Survey of the Vortex Tube, College of Aeronautics, Cranfield, Note, UK, No. 9, 1954.
[7] B.M. Dobratz, Vortex Tubes: a Bibliography, Lawrence Radiation Laboratory, UCRL-7829, April, 1964.
[8] J.M. Nash, The Ranque–Hilsch vortex tube and its application to spacecraft environmental control systems, Dev. Theor. Appl. Mech. 6 (1972).
[9] B. Ahlborn, J.U. Keller, R. Staudt, G. Treitz, E. Rebhan, Limits of temperature separation in a vortex tube, J. Phys. D: Appl. Phys. 27 (1994) 480–488.
[10] D. Schlenz, Kompressible strahlgetriebene drallstromung in rotationssymmetrischen kanalen, Ph.D. Thesis of Technische Fakultat Universitat, Erlangen-Nurnberg, 1982.
[11] T. Amitani, T. Adachi, T. Kato, A study on temperature separation in a large vortex tube, Trans. JSME 49 (1983) 877–884.
[12] W. Frohlingsdorf, H. Unger, Numerical investigations of the compressible flow and the energy separation in the Ranque–Hilsch vortex tube, Int. J. Heat Mass Transfer 42 (1999) 415–422.
[13] P. Promvong, Numerical simulation of turbulent compressible vortex-tube flow, in: Proc. of the 3rd ASME/JSME Joint Fluid Engineering, Sanfrancisco, USA, 1999.
[14] U. Behera, P.J. Paul, S. Kasthurirengan, R. Karunanithi, S.N. Ram, K. Dinesh, S. Jacob, CFD analysis and experimental investigations towards optimizing the parameters of Ranque–Hilsch vortex tube, Int. J. Heat Mass Transfer 48 (2005) 1961–1973.
[15] N.F. Aljuwayhel, G.F. Nellis, S.A. Klein, Parametric and internal study of the vortex tube using a CFD model, Int. J. Refrig. 28 (2005) 442–450.
[16] H.M. Skye, G.F. Nellis, S.A. Klein, Comparison of CFD analysis to empirical data in a commercial vortex tube, Int. J. Refrig. 29 (2006) 71–80.
[17] S. Hogg, M.A. Leschziner, Computation of highly swirling confined flow with a Reynolds stress turbulence model, AIAA J. 27 (1989) 57–63.
[18] W.P. Jones, A. Pascau, Calculation of confined swirling flows with a second moment closure, Trans. ASME, J. Fluids Eng. 111 (1989) 248–255.
[19] S. Nieh, J. Zhang, Simulation of the strongly swirling aerodynamic field in a vortex combustor, Trans. ASME, J. Fluids Eng. 114 (September) (1992).
[20] W.M. Pun, An Introduction to the TEFESS Code, Mechanical Engineering Dept., Imperial College, February, 1992.
[21] J.P. Hartnett, E.R.G. Eckert, Experimental study of the velocity and temperature distribution in a high-velocity vortex-type flow, Trans. ASME, Ser. C, J. Heat Transfer 79 (1957) 751–758.
[22] P. Promvonge, A numerical study of vortex tubes with an algebraic Reynolds stress model, Ph.D. Thesis, University of London, 1997.
[23] T.B. Gatski, Turbulent Flows: Model Equations and Solution Methodology, in: Roger Peyret (Ed.), Handbook of Computational Fluid Mechanics, Academic Press Ltd, London, 1996.
[24] C.D. Wilcox, Turbulent Modelling for CFD, DCW Industries, Inc., California, 1993.

[25] W.A. Rodi, New Algebraic Relations for Calculating the Reynolds Stresses, Z. Angew. Math. Mech. (ZAMM) 56 (1976) T219–T221.
[26] J. Zhang, S. Nieh, L. Zhou, A new version of algebraic stress model for simulating strongly swirling turbulent flows, J. Numer. Heat Transfer B 22 (1992) 49–62.
[27] S. Nieh, J. Zhang, Simulation of the strongly swirling aerodynamic field in a vortex combustor, Trans. ASME, J. Fluids Eng. 114 (1992).
[28] S.V. Patankar, Numerical Heat Transfer and Fluid Flow, Hemisphere, Washington, DC, 1980.
[29] B.P. Leonard, A stable and accurate convective modelling procedure based on quadratic upstream interpolation, Comp. Meth. Appl. Mech. Eng. 19 (1979) 59–98.
[30] T.A. Blatt, R.B. Trusch, An experimental investigation of an improved vortex cooling device, American Society of Mechanical Engineers, Winter Annual Meeting, November 1962.